

Supplementary information for: Dynamic disorder, phonon lifetimes, and the assignment of modes to the vibrational spectra of methylammonium lead halide perovskites

Aurélien M. A. Leguy¹, Alejandro R. Goñi^{2,3‡}, Jarvist M. Frost⁴, Jonathan Skelton⁴, Federico Brivio⁴, Xabier Rodríguez-Martínez², Oliver J. Weber⁴, Anuradha Pallipurath⁵, M. Isabel Alonso², Mariano Campoy-Quiles², Mark T. Weller⁴, Jenny Nelson^{1,7}, Aron Walsh⁴ and Piers R.F. Barnes^{1†}

- 1- Physics department, Imperial College London, UK, SW7 2AZ;
- 2- Institut de Ciència de Materials de Barcelona (ICMAB-CSIC), Campus UAB, 08193 Bellaterra, Spain;
- 3- ICREA, Passeig Lluís Companys 23, 08010 Barcelona, Spain ;
- 4- Chemistry department, University of Bath, UK, BA2 7AY;
- 5- School of chemistry, National University of Ireland Galway, Ireland;
- 6- SPECIFIC, College of Engineering, Swansea University, Baglan Bay Innovation and Knowledge Centre, UK, SA12 7AX;

‡ goni@icmab.es

† piers.barnes@imperial.ac.uk

List of the additional material as called in the main text:

Note S1 Detailed methods for sample preparation.

Figure S1 Variable coupling of the excitation energy to vibrational modes.

Figure S2 Assignment of the Raman features of a single crystal of MAPbI₃ at 100 K for the cage (left) and “isolated” modes (right).

Figure S3 Assignment of the Raman features of a single crystal of MAPbBr₃ at 100 K for the cage (left) and “isolated” modes (right).

Figure S4 Assignment of the Raman features of a single crystal of MAPbCl₃ at 100 K for the cage (left) and “isolated” modes (right).

Figure S5 Predicted Raman activity of MAPbI₃ in the orthorhombic, tetragonal and cubic phases.

Figure S6 Assignment of the terahertz absorbance spectrum recorded on a single crystal of MAPbI₃ at 80K.

Figure S7 Assignment of the terahertz absorbance spectrum recorded on a single crystal of MAPbI₃ at 220K.

Figure S8 Assignment of the terahertz absorbance spectrum recorded on a single crystal of MAPbI₃ at 350K.

Table S1 Theoretical modes of MAPbI₃ in the orthorhombic phase.

Figure S9 Full predicted spectrum of MAPbI₃ that takes into account the broadening due to statistical disorder.

Figure S10 Full predicted spectrum of MAPbCl₃ that takes into account the broadening due to statistical disorder.

Figure S11 Effect of disorder on the frequency of the MA torsional mode for the three halide types.

Figure S12 Assignment of the Raman features recorded on single crystals of MAPbI₃, MAPbBr₃ and MAPbCl₃ at 100 K between 800 and 1300 cm⁻¹.

Figure S13 Assignment of the Raman features recorded on single crystals of MAPbI₃, MAPbBr₃ and MAPbCl₃ at 100 K between 1400 and 1800 cm⁻¹.

Figure S14 Assignment of the Raman features recorded on single crystals of MAPbI₃, MAPbBr₃ and MAPbCl₃ at 100 K between 2750 and 3400 cm⁻¹.

Table S2 Best fit function for the Raman peaks of MAPbI₃ in its orthorhombic and tetragonal phases.

Table S3 Best fit function for the Raman peaks of MAPbBr₃ in its orthorhombic and tetragonal phases.

Table S4 Best fit function for the Raman peaks of MAPbCl₃ in its orthorhombic and tetragonal phases.

Figure S15 Temperature dependence of the Raman spectra of MAPbI₃ close to the phase transition.

Figure S16 Temperature dependence of the Raman peak positions of MAPbI₃ close to the phase transition.

Figure S17 Temperature dependence of the FWHM of characteristic Raman peaks of the three halide types.

Note S2 Method to generate disordered phonon spectra.

Note S3 Method to deduce phonon lifetimes from Raman peak broadening.

Note S1: Detailed methods for sample preparation

Methylammonium lead iodide single crystals were prepared according to the method of Poglitsch and Weber¹. 2.5 g of lead acetate trihydrate ($\text{Pb}(\text{CH}_3\text{CO}_2)_2 \cdot 3\text{H}_2\text{O}$, Sigma 99.99 %) was dissolved in 10 mL hydroiodic acid (HI_{aq} , 57 wt%, Sigma) in a 50 mL round bottom flask and heated to 100 °C in an oil bath. Separately, 0.597 g of CH_3NH_2 (aq, 40 %, Sigma) was added dropwise to a further 2 mL of HI_{aq} kept at 0 °C in an ice bath under stirring. The methylammonium iodide solution was then added to the lead acetate solution and the mixture was cooled over five days to a temperature of 46 °C, resulting in the formation of black crystals with largest face length around 8 mm. The content of the flasks was subsequently filtered and dried for 12 hours at 100 °C.

Methylammonium lead bromide single crystals were prepared using 10 mL HBr (aq, 48 wt %, Sigma) was added to 1.458 g of $\text{Pb}(\text{CH}_3\text{CO}_2)_2 \cdot 3\text{H}_2\text{O}$ in a 23 mL Teflon-lined stainless steel autoclave. Separately, 1 mL HBr was added dropwise to 0.333 mL of methylamine (aq, 40 %, Sigma) at 0 °C under stirring. The methylamine hydrobromide solution was then added to the autoclave, which was sealed and heated in a fan oven at 140 °C for 24 hours. The temperature was decreased from 140 °C to room temperature over five days. The red < 2mm crystals were filtered and dried for 12 hours at 100 °C.

Methylammonium lead chloride single crystals were prepared with 1.458 g $\text{Pb}(\text{CH}_3\text{CO}_2)_2 \cdot 3\text{H}_2\text{O}$ and 3.892 g methylamine hydrochloride (Sigma) were added to a 23 mL Teflon-lined stainless steel autoclave along with 10 mL H_2O , affording a 15:1 molar ratio $\text{Pb}(\text{CH}_3\text{CO}_2)_2 \cdot 3\text{H}_2\text{O} : \text{MA} \cdot \text{HCl}$. The reactants were heated in a fan oven at 140 °C for 24 hours. The temperature was decreased from 140 °C to room temperature over five days. The clear < 3 mm crystals were filtered and dried for 12 hours at 100 °C.

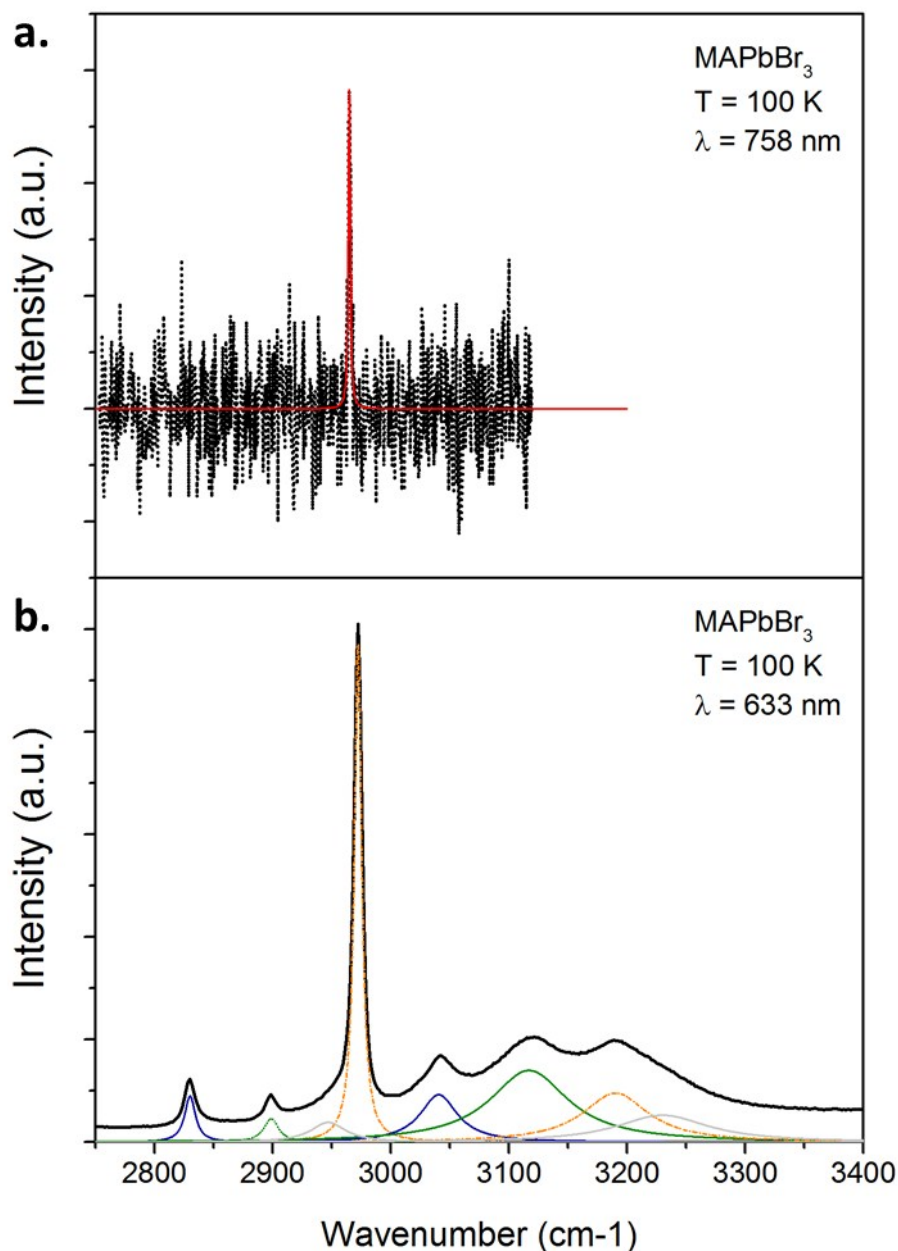


Figure S1 Variable coupling of the excitation energy to vibrational modes: Raman spectra collected on a single crystal of MAPbBr₃ at 100 K. **(a.)** Signal recorded using the 785 nm infrared excitation wavelength (solid black curve). One peak only can be identified in the noise, as can be seen on the fitted curve (solid red). **(b.)** The results of a similar experiment using the red excitation laser at 633 nm (solid black curve). In this case, 7 or 8 peaks can be resolved, as represented by the coloured fitting Lorentzian peaks.

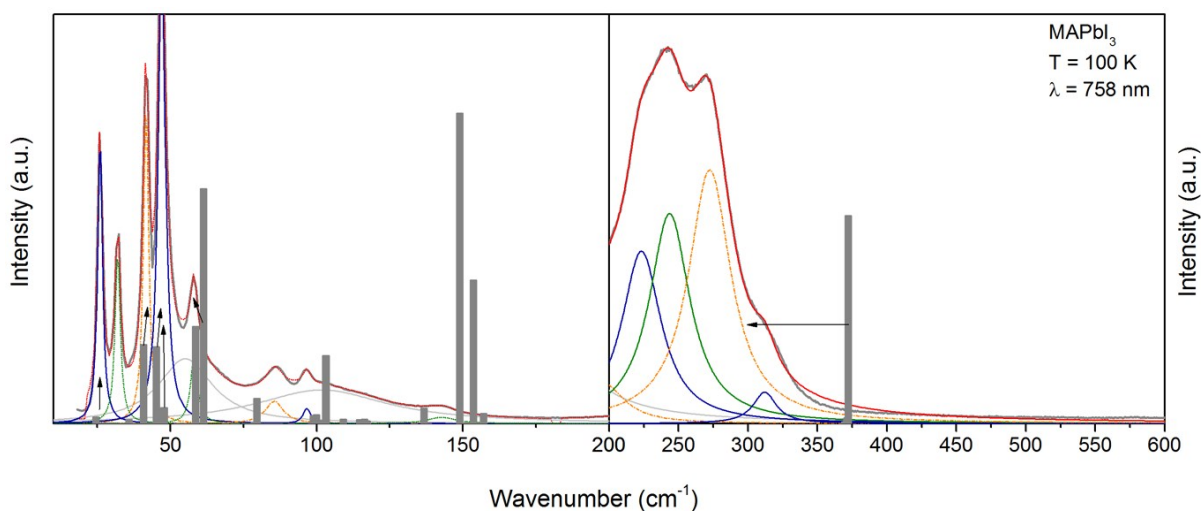


Figure S2 Assignment of the Raman features of a single crystal of MAPbI₃ at 100 K for the cage (left) and “isolated” modes (right). The solid black line is the experimental data, the solid red one is the fit obtained by summing the Lorentzian functions plotted in colours. The expected Raman active phonon modes of MAPbI₃ in the orthorhombic phase are plotted as grey bars.

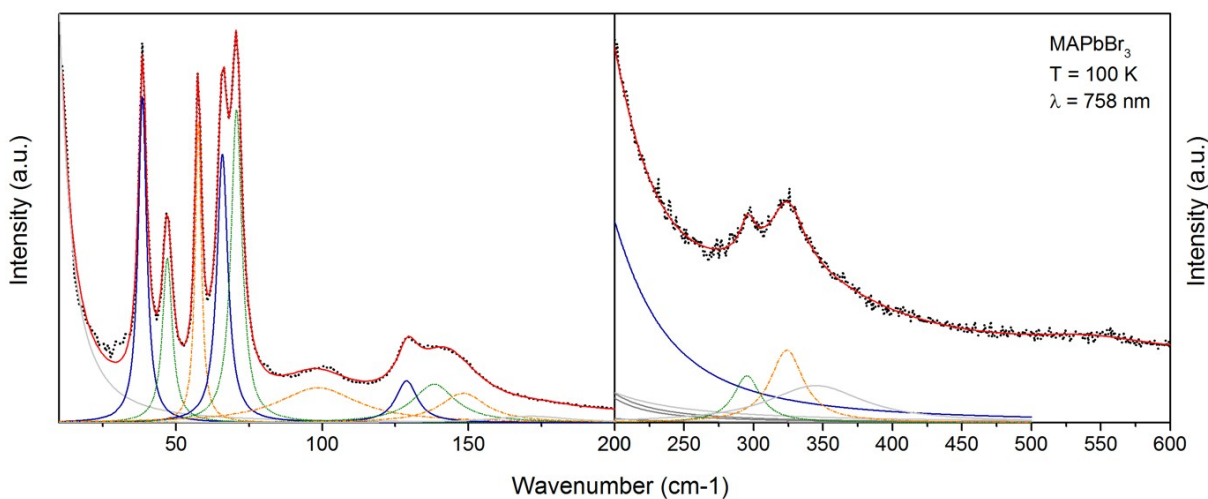


Figure S3 Assignment of the Raman features of a single crystal of MAPbBr₃ at 100 K for the cage (left) and “isolated” modes (right). The solid black line is the experimental data, the solid red one is the fit obtained by summing the Lorentzian functions plotted in colours.

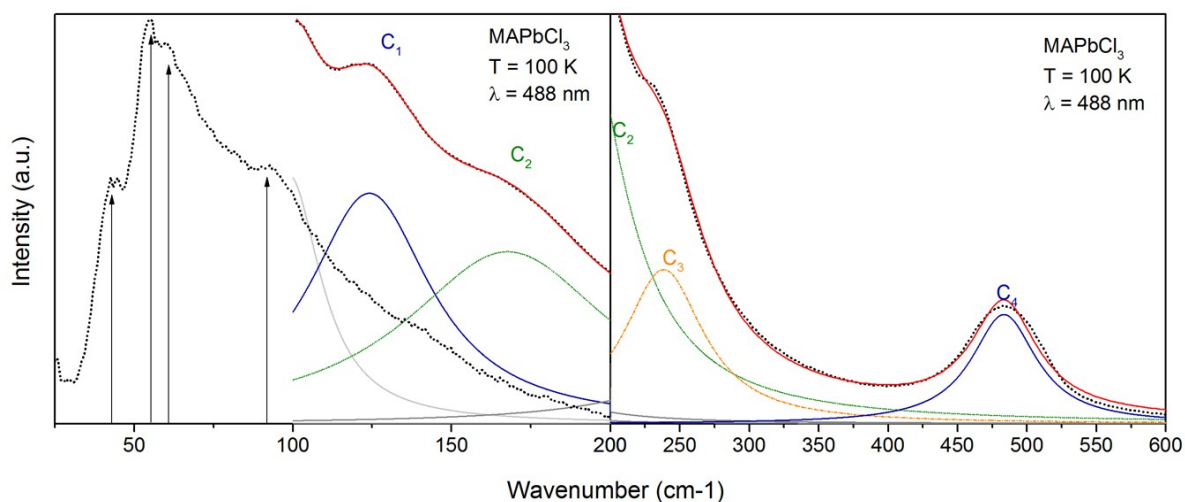


Figure S4 Assignment of the Raman features of a single crystal of MAPbCl₃ at 100 K for the cage (left) and “isolated” modes (right). The solid black line is the experimental data, the solid red one is the fit obtained by summing the Lorentzian functions plotted in colours. The dotted black line shows the lower quality spectrum recorded with the 785 nm excitation, which is measurable down to lower energies. The peak positions on the latter spectrum are shown with arrows to avoid any confusion with the data recorded with the 488 nm illumination source.

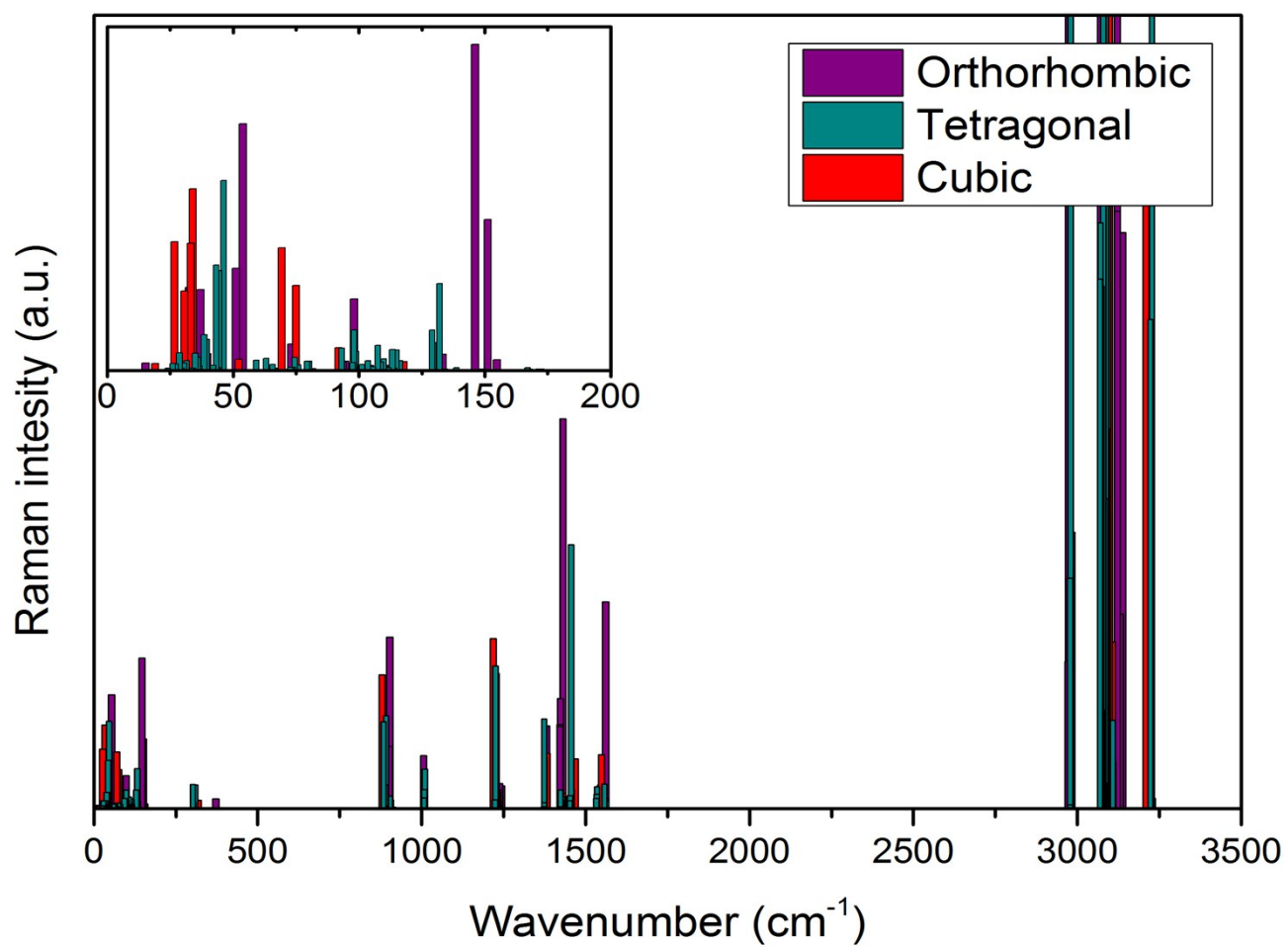


Figure S5 Predicted Raman activity of MAPbI₃ in the orthorhombic, tetragonal and cubic phases. The inset focuses on the cage modes.

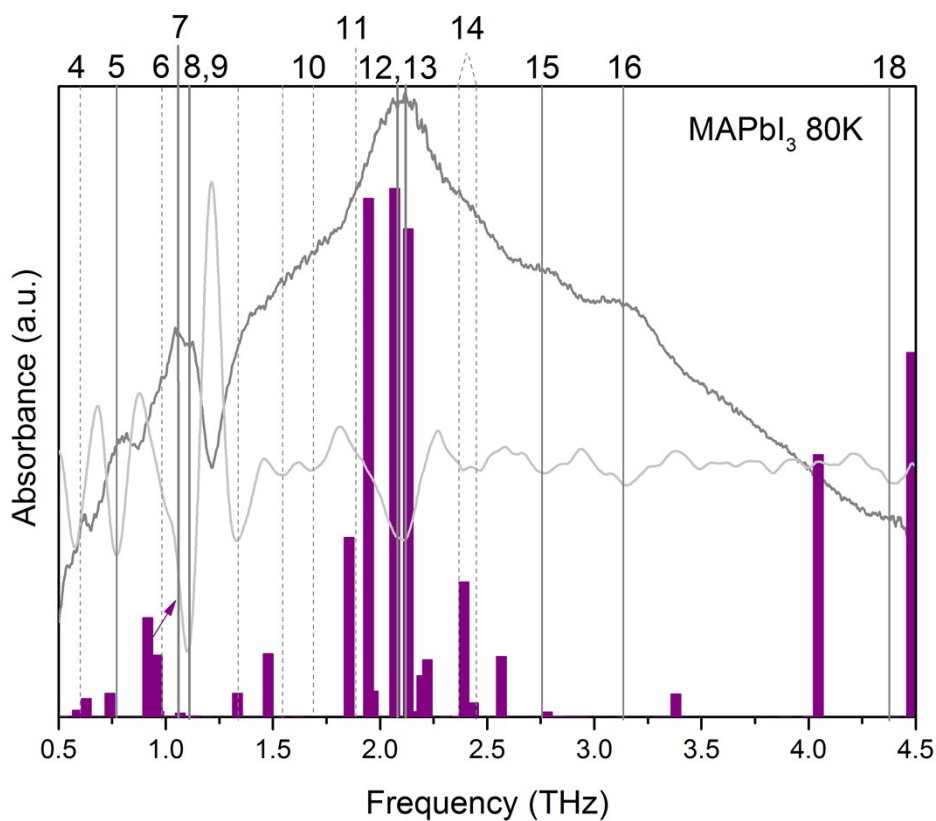


Figure S6 Assignment of the terahertz absorbance spectrum recorded on a single crystal of MAPbI_3 at 80 K. The absorbance spectrum is given in dark grey, while its second derivative is shown in a lighter shade. The second derivative was obtained by differentiating the smoothed absorption spectrum using the Savitzky-Golay method.² The dips of the second derivative pinpoint the features. The expected infrared active modes in the orthorhombic phase are given as purple bars. Lines are used to highlight the main features (solid lines for the clearest ones, dotted lines when the position is less clear). The numbers on top of the lines are the corresponding theoretical modes (see **Table 1** in the main text).

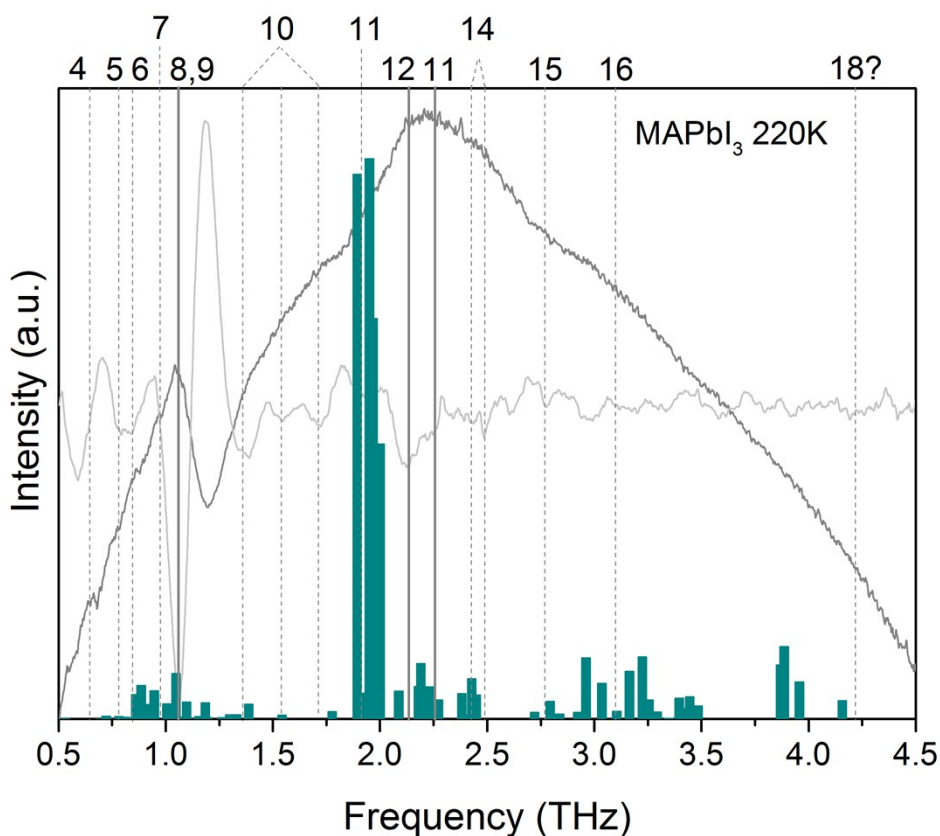


Figure S7 Assignment of the terahertz absorbance spectrum recorded on a single crystal of MAPbI₃ at 220 K. The absorbance spectrum is given in dark grey, while its second derivative is shown in a lighter shade. The second derivative was obtained by differentiating the smoothed absorption spectrum using the Savitzky-Golay method.² The dips of the second derivative pinpoint the features. The expected infrared active modes in the tetragonal phase are given as dark cyan bars. Lines are used to highlight the main features (solid lines for the clearest ones, dotted lines when the position is less clear). The numbers on top of the lines are the corresponding theoretical modes (see **Table 1** in the main text).

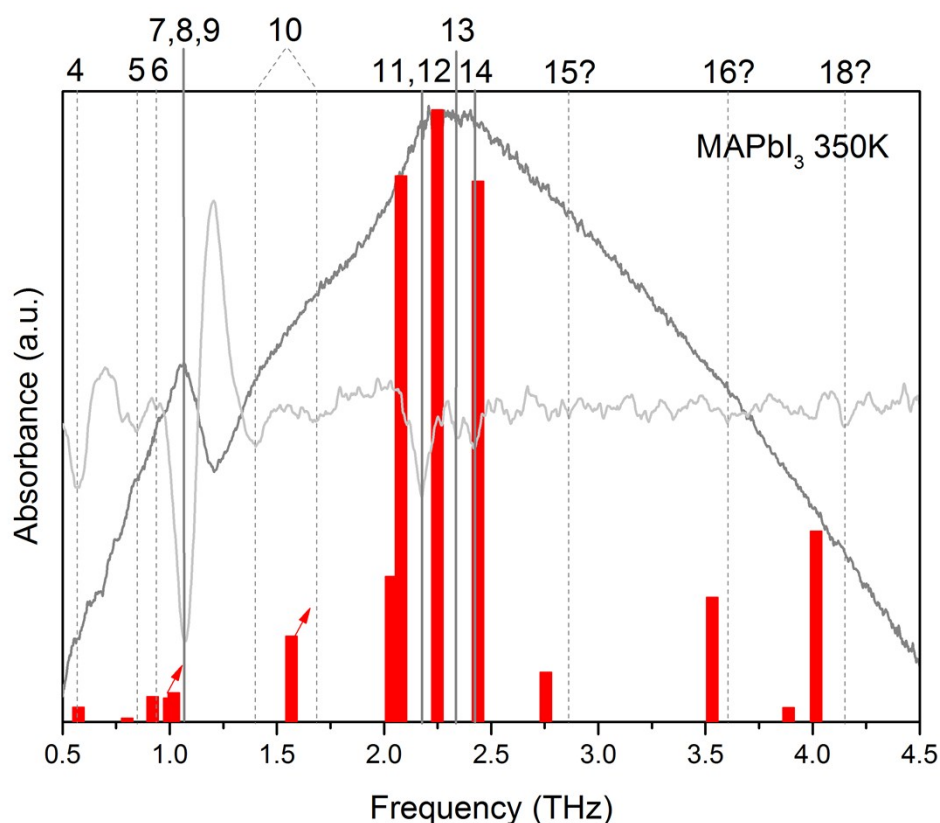


Figure S8 Assignment of the terahertz absorbance spectrum recorded on a single crystal of MAPbI₃ at 350 K. The absorbance spectrum is given in dark grey, while its second derivative is shown in a lighter shade. The second derivative was obtained by differentiating the smoothed absorption spectrum using the Savitzky-Golay method.² The dips of the second derivative pinpoint the features. The expected infrared active modes in the cubic phase are given as red bars. Lines are used to highlight the main features (solid lines for the clearest ones, dotted lines when the position is less clear). The numbers on top of the lines are the corresponding theoretical modes (see **Table 1** in the main text).

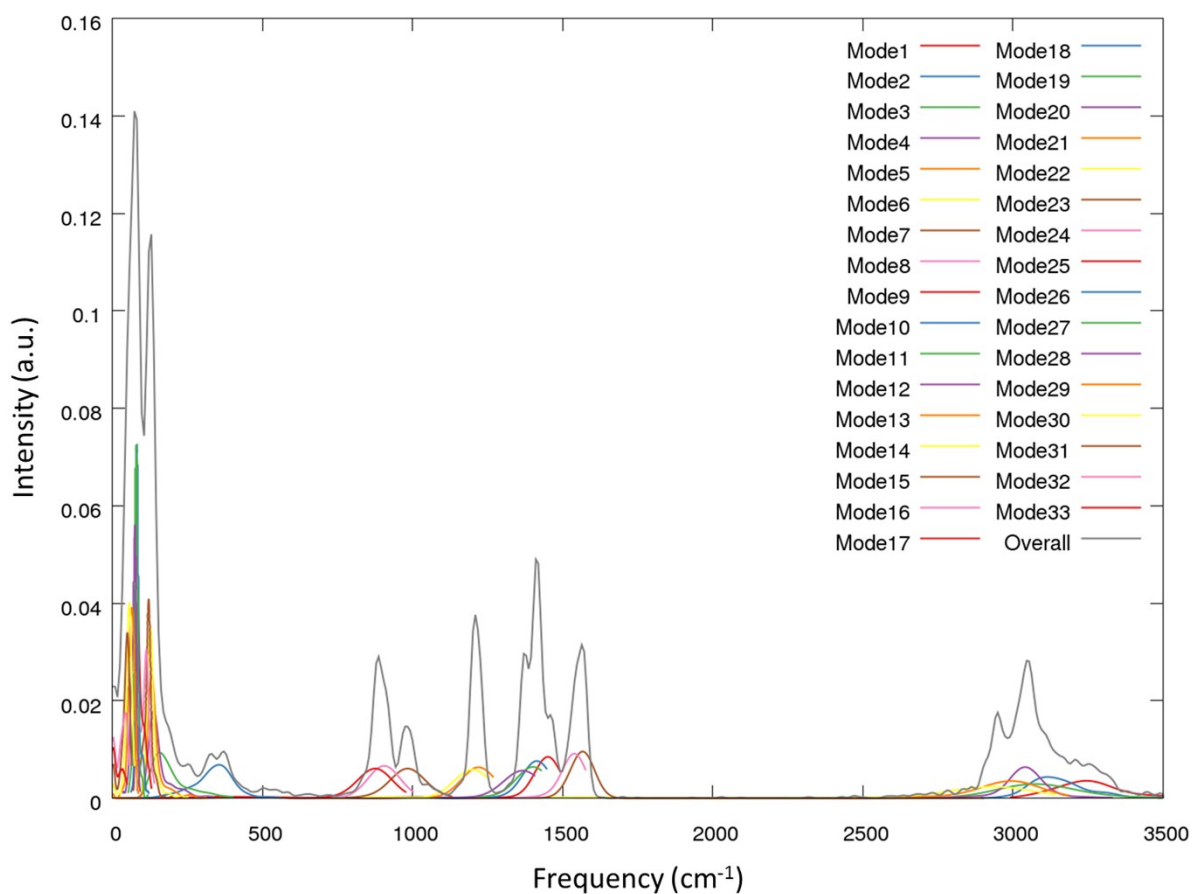


Figure S9 Full predicted spectrum of MAPbI₃ that takes into account the broadening due to statistical disorder.

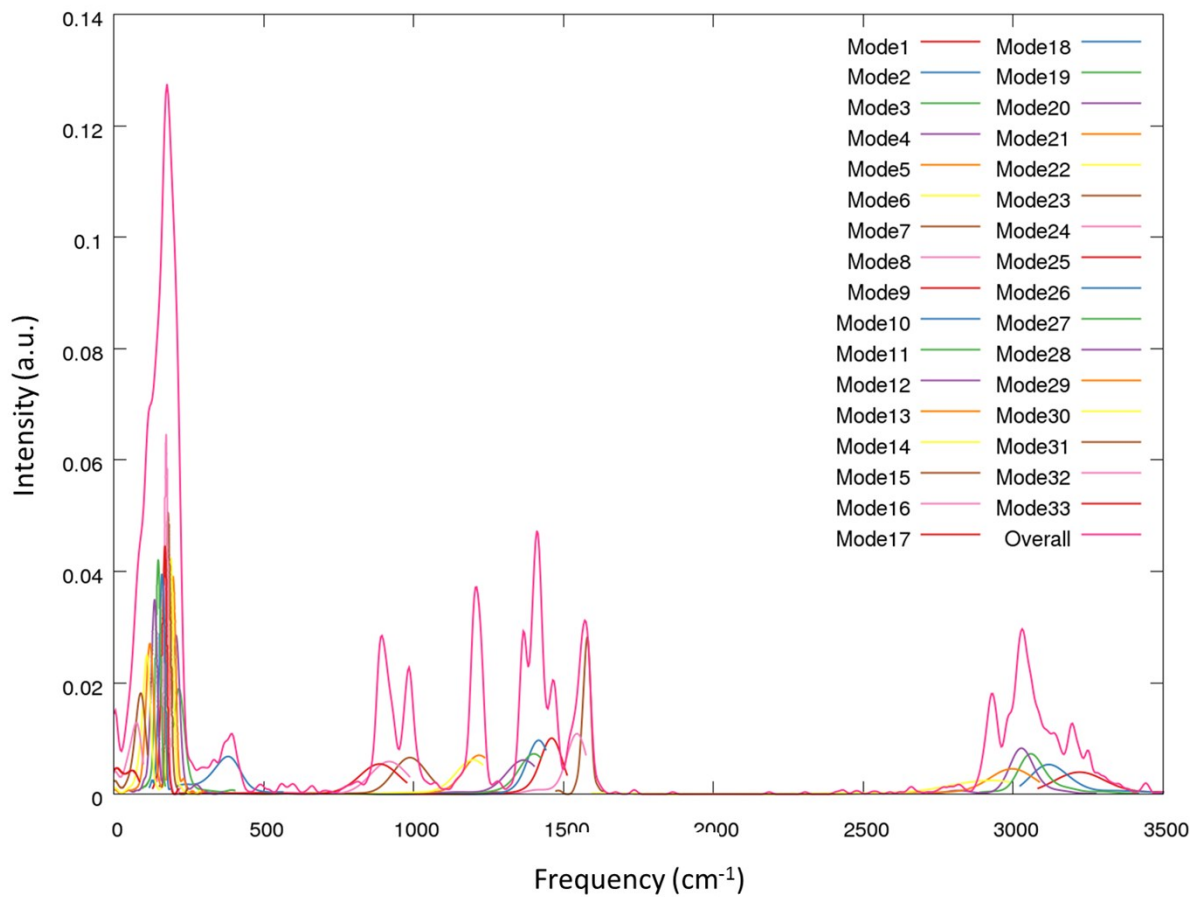


Figure S10 Full predicted spectrum of MAPbCl₃ that takes into account the broadening due to statistical disorder.

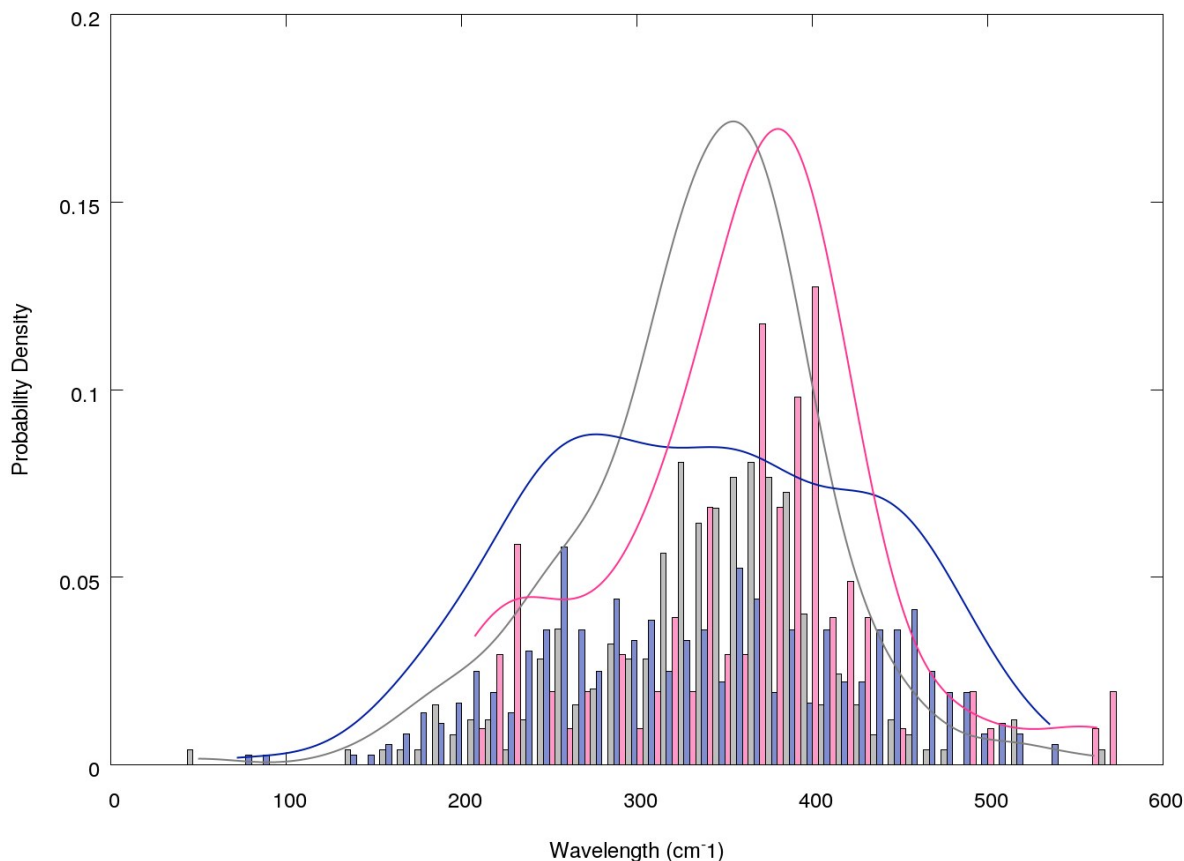


Figure S11 Effect of disorder on the frequency of the MA torsional mode (19 in **Figure 3** and **Table 3**) of MAPbI₃ (grey), MAPbBr₃ (blue) and MAPbCl₃ (pink). The histograms show the distribution of frequencies of mode 19, extracted from 248 individual calculations in which the MA cation was randomly orientated and partially relaxed (see supplementary information). The solid line is the kernel density estimation of these sampled data.

Table S1 Theoretical modes of MAPbI₃ in the orthorhombic phase, from Ref.³ The 17 most active cage modes are bolded (activity higher than 10 A⁴ amu⁻¹).

Mode #	ν / cm ⁻¹	ν / THz	IR Activity / A ² e ²	Raman Activity / A ⁴ amu ⁻¹
73	154.81	4.64	1.89E-07	2.50E+01
74	154.10	4.62	4.45E-02	4.83E-03
75	152.05	4.56	2.32E-02	4.68E-01
76	151.15	4.53	9.52E-05	3.51E+02

77	150.62	4.52	1.97E-06	1.32E+00
78	149.47	4.48	4.62E-01	4.33E-01
79	149.00	4.47	9.60E-06	2.54E+00
80	146.81	4.40	3.47E-05	3.66E-01
81	146.17	4.38	2.06E-04	7.58E+02
82	134.92	4.04	3.33E-01	1.98E-01
83	133.36	4.00	4.10E-04	3.76E+01
84	129.89	3.89	1.41E-08	1.34E-01
85	113.09	3.39	6.56E-08	4.89E-01
86	112.85	3.38	4.75E-06	6.48E+00
87	112.77	3.38	2.93E-02	3.39E-02
88	111.98	3.36	6.70E-05	1.15E+01
89	111.11	3.33	4.77E-07	4.23E+00
90	110.18	3.30	2.47E-07	9.51E+00
91	104.35	3.13	9.39E-09	1.13E+01
92	98.05	2.94	1.92E-06	1.66E+02
93	96.46	2.89	1.89E-09	7.87E+00
94	96.21	2.88	6.49E-09	5.67E+00
95	94.62	2.84	3.38E-05	2.15E+01
96	94.47	2.83	6.47E-04	7.96E-01
97	93.61	2.81	8.02E-06	1.99E+01
98	92.74	2.78	6.48E-03	7.52E-02
99	85.59	2.57	7.70E-02	1.63E-02
100	81.27	2.44	1.81E-02	2.11E-03
101	79.78	2.39	1.71E-01	1.49E-02
102	78.85	2.36	9.22E-04	1.21E-02
103	76.82	2.30	4.43E-08	3.33E-03
104	74.09	2.22	7.27E-02	5.44E-01
105	73.22	2.20	5.24E-02	1.86E+00
106	73.15	2.19	3.96E-04	6.12E+01
107	72.26	2.17	6.72E-03	3.18E+00
108	71.11	2.13	6.19E-01	4.41E-02
109	70.34	2.11	4.60E-06	3.81E-03
110	69.01	2.07	6.70E-01	3.87E-03

111	65.88	1.98	1.02E-07	5.20E-04
112	65.62	1.97	3.27E-02	2.80E-01
113	64.92	1.95	6.58E-01	2.79E-02
114	61.91	1.86	2.28E-01	7.71E-04
115	53.97	1.62	3.35E-05	5.74E+02
116	51.22	1.54	3.27E-05	2.37E+02
117	49.30	1.48	8.06E-02	5.99E-02
118	46.92	1.41	3.31E-07	4.20E-02
119	44.54	1.34	3.02E-02	2.29E-02
120	39.80	1.19	8.88E-07	3.90E+01
121	37.78	1.13	1.09E-07	2.29E+00
122	37.76	1.13	1.63E-03	3.29E-02
123	37.00	1.11	4.02E-06	1.88E+02
124	35.62	1.07	5.15E-03	2.04E-03
125	34.29	1.03	1.19E-06	1.68E+00
126	33.79	1.01	1.38E-07	5.22E-03
127	32.39	0.97	9.40E-05	1.93E+02
128	32.27	0.97	7.26E-03	5.80E-01
129	32.03	0.96	7.88E-02	1.72E-01
130	30.53	0.92	1.26E-01	4.69E-02
131	28.63	0.86	2.40E-07	7.63E-03
132	28.15	0.84	3.78E-06	6.57E-03
133	27.22	0.82	2.58E-04	1.01E+01
134	24.66	0.74	3.03E-02	6.23E-04
135	23.51	0.70	3.09E-06	4.46E-01
136	22.49	0.67	1.65E-06	1.24E-02
137	20.98	0.63	2.34E-02	1.15E-01
138	19.60	0.59	8.82E-03	6.63E-02
139	17.35	0.52	4.81E-04	5.51E-03
140	16.76	0.50	1.05E-07	4.12E-03
141	15.31	0.46	5.29E-06	1.68E+01
142	0.18	0.01	3.83E-07	-
143	0.28	0.01	1.46E-07	-
144	0.41	0.01	4.97E-07	-

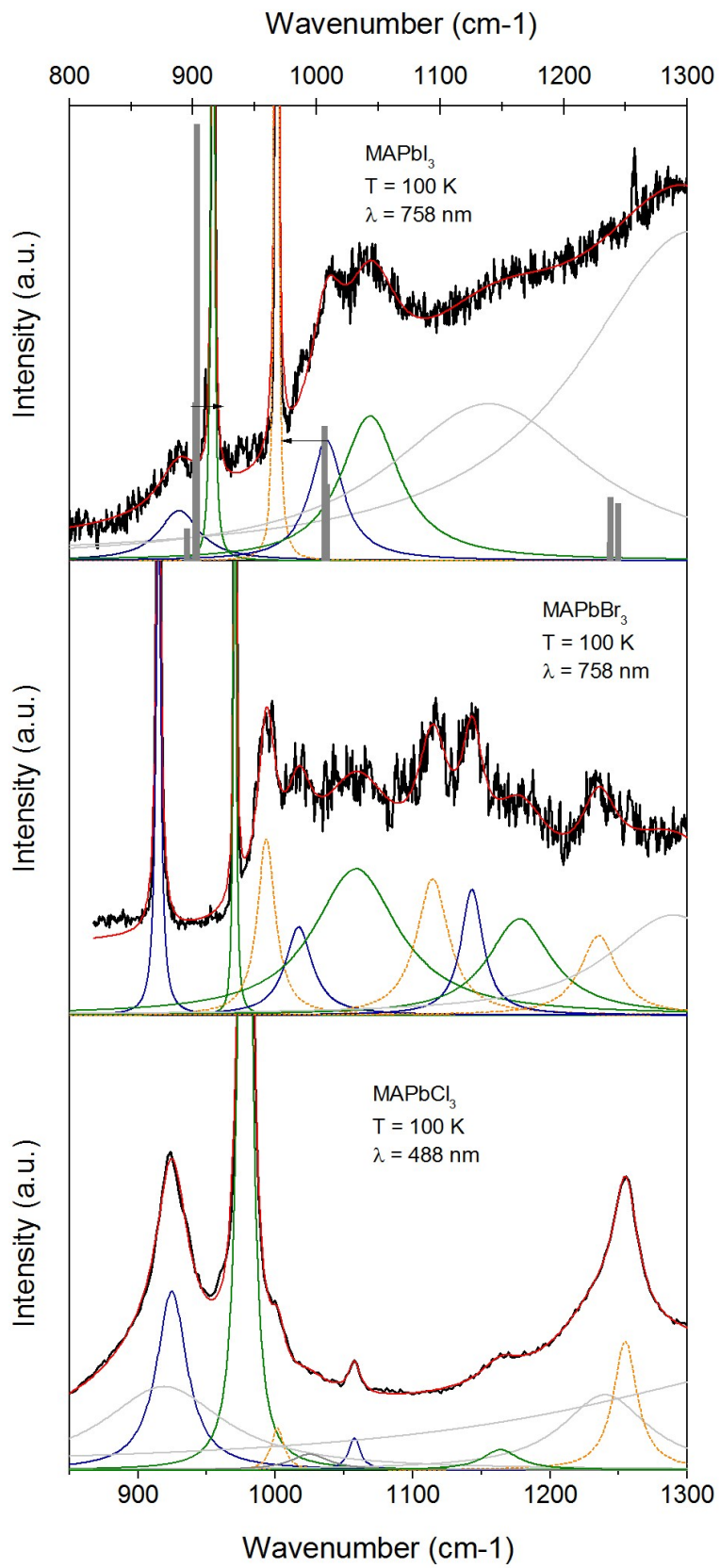


Figure S12 Assignment of the Raman features recorded on single crystals of MAPbI₃, MAPbBr₃ and MAPbCl₃ at 100 K between 800 and 1300 cm⁻¹. The solid black lines are the experimental spectra; the solid red ones are the fit obtained by summing the Lorentzian functions plotted in colours. The expected Raman active phonon modes of MAPbI₃ in the orthorhombic phase are plotted as grey bars.

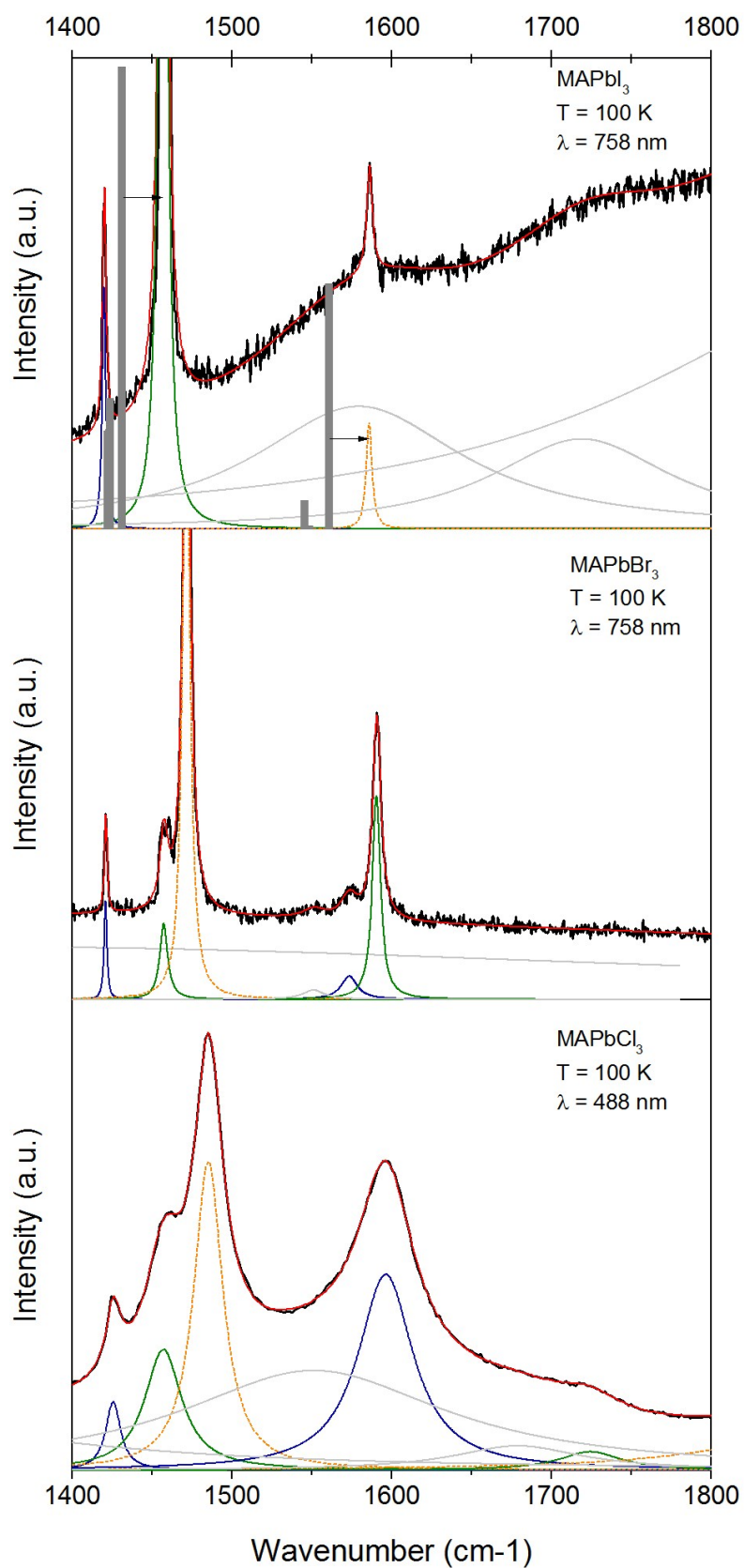


Figure S13 Assignment of the Raman features recorded on single crystals of MAPbI_3 , MAPbBr_3 and MAPbCl_3 at 100 K between 1400 and 1800 cm^{-1} . The solid black lines are the experimental spectra; the solid red ones are the fit obtained by summing the

Lorentzian functions plotted in colours. The expected Raman active phonon modes of MAPbI_3 in the orthorhombic phase are plotted as grey bars.

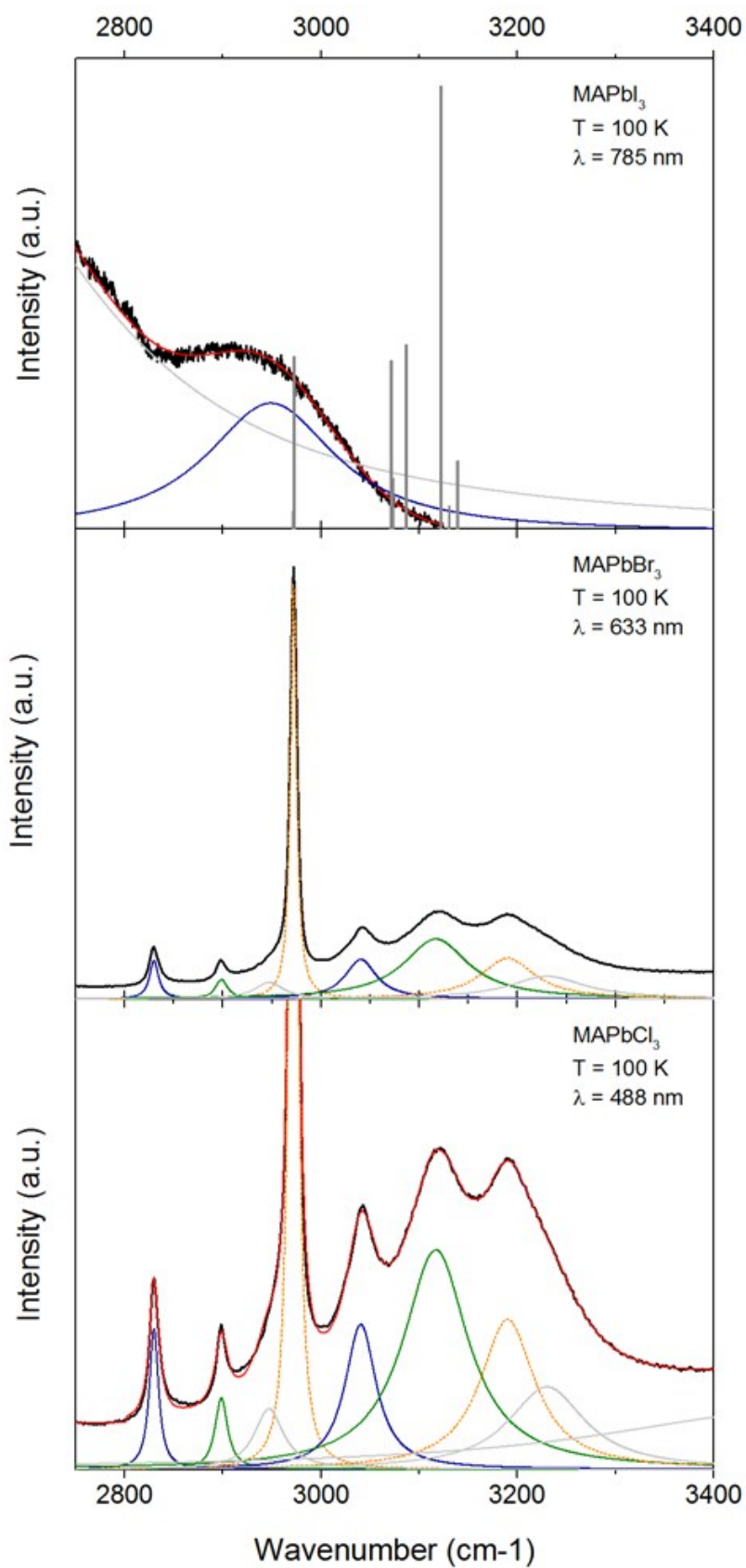


Figure S14 Assignment of the Raman features recorded on single crystals of MAPbI₃, MAPbBr₃ and MAPbCl₃ at 100 K between 2750 and 3400 cm⁻¹. The solid black lines are the experimental spectra; the solid red ones are the fit obtained by summing the Lorentzian or Gaussian functions plotted in colours. The expected Raman active phonon modes of MAPbI₃ in the orthorhombic phase are plotted as grey bars.

Table S2 Best fit function for the Raman peaks of MAPbI₃ in its orthorhombic and tetragonal phases.

Mode cm⁻¹ at 100 K	Orthorhombic 100 K	Tetragonal 300K
26	Lorentzian	Gaussian
32	Lorentzian	Gaussian
42	Lorentzian	Gaussian
58	Lorentzian	Lorentzian
86	Lorentzian	Lorentzian
97	Lorentzian	Lorentzian
143	Lorentzian	Lorentzian
312	Lorentzian	Lorentzian
889	Lorentzian	Lorentzian
916	Lorentzian	Lorentzian
968	Lorentzian	Lorentzian
1008	Lorentzian	Lorentzian
1043	Lorentzian	Lorentzian
1420	Lorentzian	Lorentzian
1457	Lorentzian	Lorentzian
1586	Gaussian	Gaussian
2949	Gaussian	Gaussian

Table S3 Best fit function for the Raman peaks of MAPbBr₃ in its orthorhombic, tetragonal and cubic phases.

Mode cm⁻¹	Orthorhombic	Tetragonal	Cubic
-----------------------------	---------------------	-------------------	--------------

at 100 K	100 K	200K	300K
39	Lorentzian	Gaussian	Gaussian
47	Lorentzian	Gaussian	Gaussian
66	Lorentzian	Gaussian	Gaussian
71	Lorentzian	Gaussian	Gaussian
99	Lorentzian	Gaussian	Gaussian
138	Lorentzian	Lorentzian	Lorentzian
148	Lorentzian	Lorentzian	Lorentzian
326	Lorentzian	Lorentzian	Lorentzian
915	Lorentzian	Lorentzian	Lorentzian
970	Lorentzian	Lorentzian	Lorentzian
994	Lorentzian	Lorentzian	Lorentzian
1017	Lorentzian	Lorentzian	Lorentzian
1059	Lorentzian	Lorentzian	Lorentzian
1115	Lorentzian	Lorentzian	Lorentzian
1143	Lorentzian	Lorentzian	Lorentzian
1178	Lorentzian	Lorentzian	Lorentzian
1236	Lorentzian	Lorentzian	Lorentzian
1421	Lorentzian	Lorentzian	Lorentzian
1458	Lorentzian	Lorentzian	Lorentzian
1471	Lorentzian	Lorentzian	Lorentzian
1573	Lorentzian	Lorentzian	Lorentzian
1590	Lorentzian	Lorentzian	Lorentzian
2821	Lorentzian	Lorentzian	Lorentzian
2896	Lorentzian	Lorentzian	Lorentzian
2965	Lorentzian	Lorentzian	Lorentzian
3033	Lorentzian	Lorentzian	Lorentzian
3106	Lorentzian	Lorentzian	Lorentzian
3144	Lorentzian	Lorentzian	Lorentzian
3179	Lorentzian	Lorentzian	Lorentzian

Table S4 Best fit function for the Raman peaks of MAPbCl₃ in its orthorhombic and cubic phases.

Mode cm⁻¹ at 100 K	Orthorhombic 100 K	Cubic 300K
43	Lorentzian	Lorentzian
55	Lorentzian	Lorentzian
61	Lorentzian	Lorentzian
92	Lorentzian	Lorentzian
124	Lorentzian	Lorentzian
168	Lorentzian	Lorentzian
238	Lorentzian	Lorentzian
483	Lorentzian	Lorentzian
925	Lorentzian	Lorentzian
978	Lorentzian	Lorentzian
1002	Lorentzian	Lorentzian
1058	Lorentzian	Lorentzian
1164	Lorentzian	Lorentzian
1255	Lorentzian	Lorentzian
1425	Lorentzian	Lorentzian
1457	Lorentzian	Lorentzian
1485	Lorentzian	Lorentzian
1596	Lorentzian	Lorentzian
2830	Lorentzian	Lorentzian
2899	Lorentzian	Lorentzian
2972	Lorentzian	Lorentzian
3040	Lorentzian	Lorentzian
3117	Lorentzian	Lorentzian
3190	Lorentzian	Lorentzian

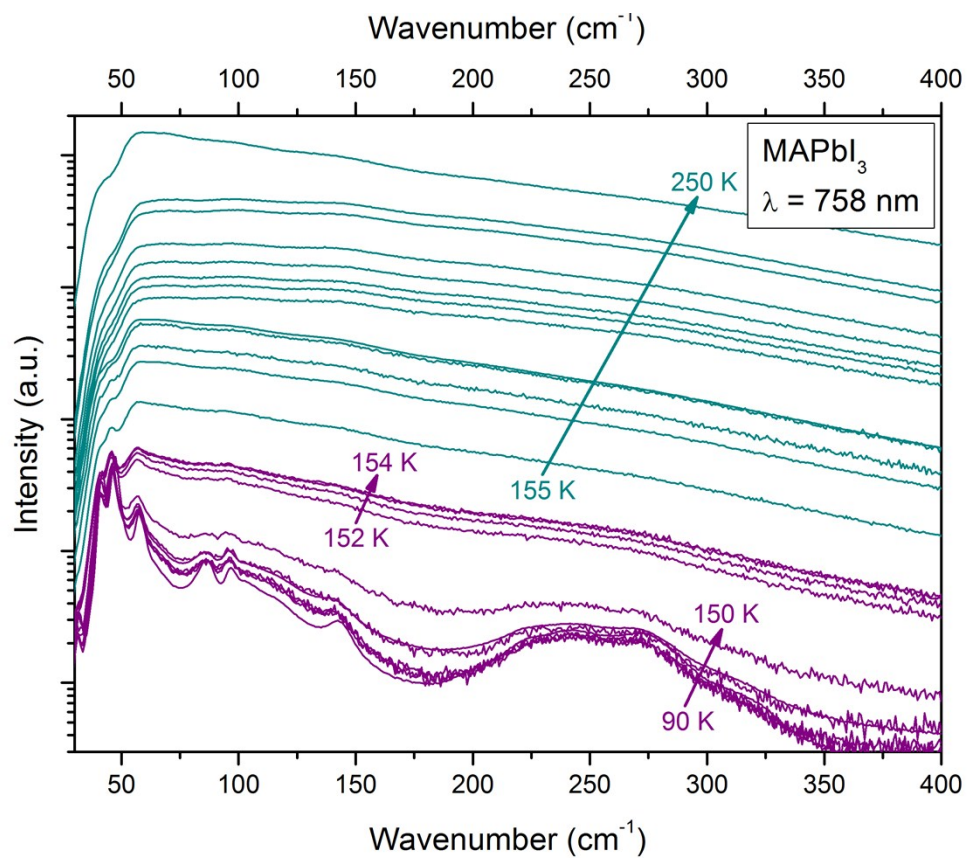


Figure S15 Temperature dependence of the Raman spectra of MAPbI₃ close to the phase transition. The colour code is the same as in **Figure 1** in the main text. The data is reported for the excitation wavelength $\lambda = 785$ nm, which yields the clearest data.

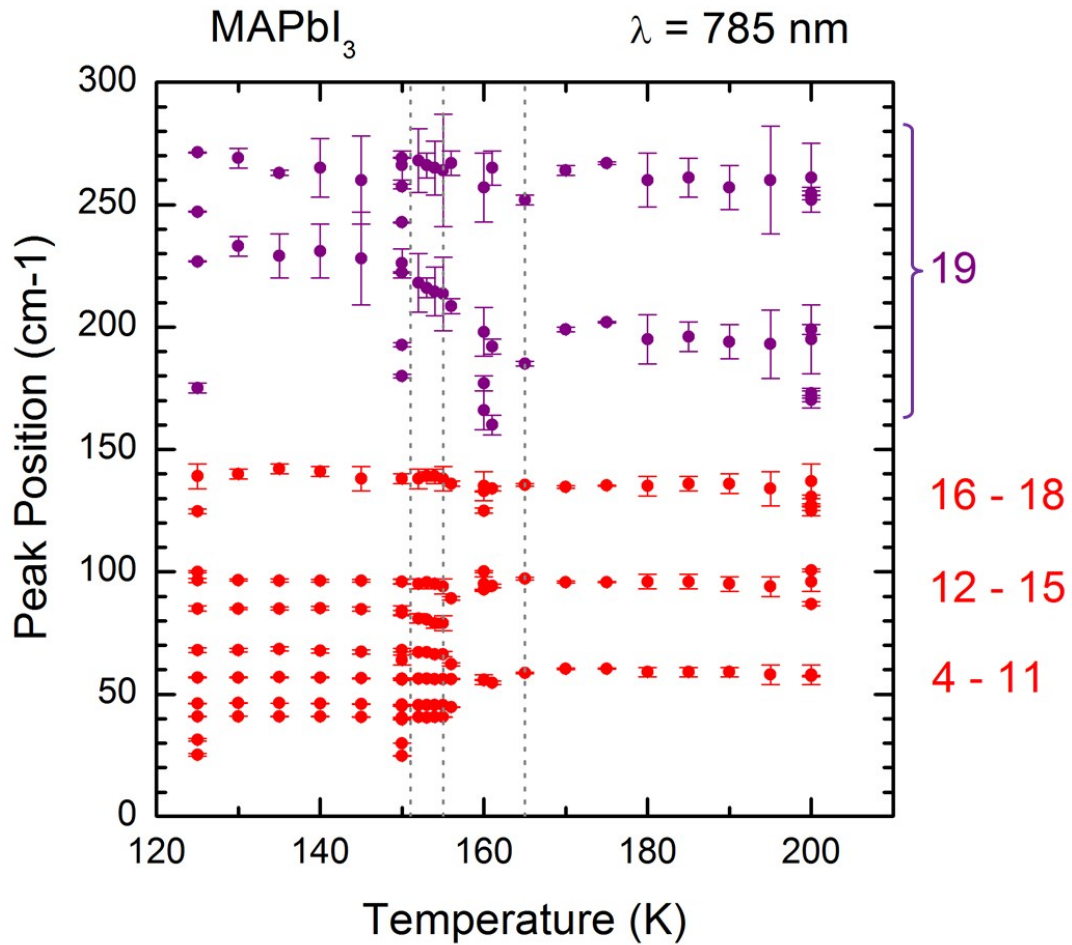


Figure S16 Temperature dependence of the Raman peak positions of MAPbI₃ close to the phase transition. The colour code is the same as in **Figure 1** in the main text. The data is reported for the excitation wavelength $\lambda = 785$ nm, which yields the clearest data. The assignment of the Raman peaks is given above the order-disorder phase transition (see **Figure 5** in the main text for a description of the labels).

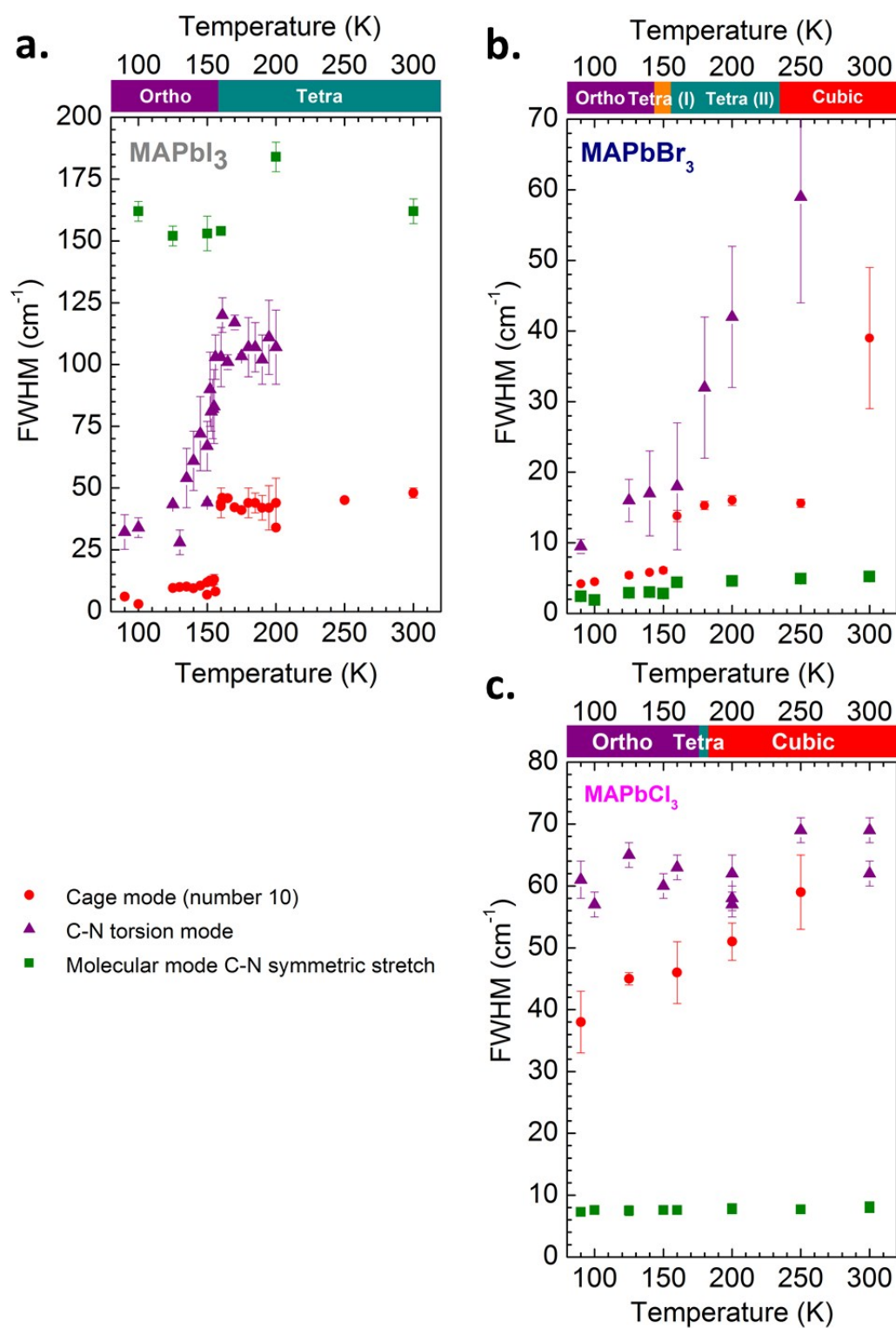


Figure S17 Temperature dependence of the FWHM of typical Raman peaks for MAPbI₃ (a.), MAPbBr₃ (b.) and MAPbCl₃ (c.). The green square markers show a typical molecular mode for each compound (here the C-H symmetric stretch, see **Table 3** in the main text), the red circle markers a cage mode (mode number 10, see **Tables 1**

and 2 in the main text), and the purple triangles represent the C-N torsion mode (i.e. the isolated mode, see **Table 3** in the main text).

Note S2: Method to generate disordered phonon spectra

The width of the vibrations as measured by Raman spectroscopy can be directly related to the phonon lifetimes. These in turn come from the anharmonic contributions to the dynamic matrix - harmonic phonons have an infinite lifetime, their Raman response should be perfectly sharp. Direct calculation of these lifetimes will be the subject of a future work. Such homogenous broadening should result in a Lorentzian form to the peak shape as observed by Raman scattering, as is the case below the orthorhombic phase transition temperature for all three halides.

An additional source of peak width is the disorder induced by thermal motion. In the high temperature modes of these methylammonium perovskites, it is believed that the methylammonium rotates. There is some evidence that the tetragonal phase has mostly two dimensional disorder in the methyl-ammonium direction, continuously converting to full three dimensional disorder once in the cubic phase.

In order to understand the influence on such disorder in the methylammonium orientation on the vibration spectra, we undertake a series of ab-initio calculations. Starting with our carefully optimised pseudo-cubic phase. The methylammonium is rotated randomly (using a Quaternion rotation matrix representation, populated with four normally distributed pseudo-random numbers), and displaced by a normally distributed vector with standard deviation 0.3 Å. From this randomly orientated structure, a conjugate gradient energy minimisation algorithm is followed for a maximum of 101 steps. The Hessian is then calculated from Density-Functional Perturbation Theory (DFPT) and diagonalised to produce frequencies and eigenvectors. For computational tractability, the size of basis set is severely reduced. Calculations are carried out at the Gamma point with the same 700 eV plane cut-off as was found for convergence in the more considered calculations. The many realisations of disorder, tempered by the conjugate gradient energy relaxation, are then used to build histograms of the distribution of frequencies as a result of inhomogeneous broadening.

Note S3: methodology to extract phonon lifetimes from peak broadening

The natural width of the Raman peaks is deconvolved from the instrumental broadening using the method developed by Olivero and Longbothum⁴ assuming that the measured FWHM is given by:

$$FWHM = 0.5346\omega_L + \sqrt{0.2166\omega_L^2 + \omega_G^2}$$

where ω_L is the natural (Lorentzian) width to be determined and ω_G the Gaussian width introduced by the apparatus. A value of $\omega_G = 2.6 \text{ cm}^{-1}$ was measured on a single crystal of Si with the same settings than the other Raman measurements reported in this study. Values of ω_L were extracted by selecting the positive root of the quadratic equation.

The phonon lifetime associated to a Lorentzian profile is proportional to $1/FWHM$. In the case of Gaussian profiles, only the lower limit of the lifetime can be estimated: since a Gaussian is the superposition of a continuum of Lorentzians, its FWHM is larger or equal to the FWHM of the Lorentzians. The value extracted with the method above corresponds therefore to a lower limit of the phonon lifetime.

References:

1. A. Poglitsch and D. Weber, *The Journal of Chemical Physics*, 1987, **87**, 6373-6378.
2. A. Savitzky and M. J. E. Golay, *Analytical Chemistry*, 1964, **36**, 1627-1639.
3. F. Brivio, J. M. Frost, J. M. Skelton, A. J. Jackson, O. J. Weber, M. T. Weller, A. R. Goni, A. M. A. Leguy, P. R. F. Barnes and A. Walsh, *Phys. Rev. B*.
4. J. J. Olivero and R. L. Longbothum, *Journal of Quantitative Spectroscopy and Radiative Transfer*, 1977, **17**, 233-236.